



PCCP

Characterization of three phases of liquid carbon by tight-binding molecular dynamics simulations

Journal:	<i>Physical Chemistry Chemical Physics</i>
Manuscript ID	CP-ART-04-2020-001875.R1
Article Type:	Paper
Date Submitted by the Author:	20-May-2020
Complete List of Authors:	Cheng, Rong; Qingdao University, College of Physics and State Key Laboratory of Bio-Fibers and Eco-Textiles Lu, Wen-Cai; Qingdao University, College of Physics and State Key Laboratory of Bio-Fibers and Eco-Textiles Ho, Kai Ming; Ames Laboratory-U.S. DOE; Iowa State University, Physics and Astronomy Wang, Cai Zhuang; Ames Laboratory-U.S. DOE; Iowa State University, Physics and Astronomy

SCHOLARONE™
Manuscripts

Characterization of three phases of liquid carbon by tight-binding molecular dynamics simulations

Rong Cheng,^{1,2} Wen-Cai Lu,^{1,2} K. M. Ho² and C. Z. Wang^{2†}

¹*College of Physics and State Key Laboratory of Bio-Fibers and Eco-Textiles, Qingdao University, Qingdao, Shandong 266071, China*

²*Ames Laboratory-U.S. DOE and Department of Physics and Astronomy, Iowa State University, Ames, IA 50011, U.S.A*

Abstract

We have performed systematic molecular dynamics simulations to study the structures of liquid carbon at 5000K with the weight density ranging from 1.4 to 3.5g/cm³, using a three-center tight-binding potential of carbon. The simulation results show the bonding characteristics in the liquid changes predominately from twofold to threefold, and then to fourfold coordination as the density increases. Signals of two structural changes at the density about 1.9 and 3.0g/cm³ respectively are revealed by the slope changes in the density dependence of structural, electronic and dynamical properties. Our simulation results suggest that there are three distinct liquid carbon phases in this density range. However, further thermodynamics calculations, e.g., free energy calculations, would be required to clarify the possible liquid-liquid transitions.

I. Introduction

The capability of carbon to have variable oxidation states or coordination number makes it one of the few elements to have multiple numbers of allotropic forms. The valence electrons of a carbon atom consists of two *s* and four *p* electrons which can form strong *sp*, *sp*² or *sp*³ chemical bonds with other carbon atoms. Such a unique bonding characteristics leads to the formation of various allotropes of solid carbon (crystalline or amorphous). The known solid allotropes include diamond, graphite, graphene, fullerene, nanotube, and carbyne etc. These carbon allotropes have attracted tremendous interests due to their intriguing physical and chemical properties and potential useful applications in modern technologies.

Since liquid is a fundamental phase of matter, it is of great interest to explore how the unique ability of carbon to catenate in various forms manifests in the structures and properties of its liquid phase. According to various estimated phase diagrams of carbon, carbon liquid can exist only at very high temperature (>4500K) and the melting temperature would further increase with applied pressure [1]. Therefore, direct measurement of the structures and properties of liquid carbon (*l*-C) by experiments remains an outstanding challenge. On the other hand, accurate and reliable theoretical studies, mainly computer simulations, can provide useful insights into the structures and properties of

liquid carbon at atomic level. Indeed, a large amount of computer simulations using molecular dynamics (MD), have greatly advanced the general understanding of the structures and properties of *l*-C [2-11].

As early as 1989, Galli *et al.* investigated the atomic and bonding properties of *l*-C at a density of 2g/cm^3 and at 5000K, using a first-principles MD method [4, 5]. They showed that the liquid in this condition is metallic composed of twofold, threefold and fourfold coordinated atoms. In 1996, Grumbach and Martin also performed first-principles MD simulations to study the structures and properties of *l*-C but focused on high pressure regime (400Gpa and above) [6]. In 1999, Glosli and Ree studied the *l*-C in 5500K to 9000K temperature range and in 0 to 20GPa pressure interval, using MD simulations based on the Brenner's classical bond-order potential [7]. They showed that the low-density liquid phase is dominated by *sp*-bonded atoms with very little *sp*³ hybridized atoms, while the high-density liquid phase contains mostly *sp*³-bonded atoms with very little *sp* hybridized atoms. They also illuminated that the lack of *sp*²-bonded atoms is due to a large torsional energy barrier and a low entropy relative to the $\sigma\pi$ bond. However, the lack of *sp*² bonding is in disagreement with the results of the subsequent first-principles MD and tight-binding (TB) MD simulations [8-10]. Wu *et al.* performed first-principles MD simulations to investigate the *l*-C as a function of density along 6000K isotherm [8]. The simulation results show a continuous evolution from a low-density primarily *sp*-like liquid to an intermediate-density *sp*²-like and then a high-density *sp*³-like liquid, with *sp*² sites being present at all densities (from 1.27 to 3.02g/cm^3). They also concluded that the discrepancy between quantum and classical simulations can be attributed to the deficiency in Brenner's bond-order potential to describe lone pair electrons. Subsequently, another density-functional based molecular dynamics simulations using the Car-Parrinello method with the Becke exchange and Perdew correlation gradient corrected functional showed that *l*-C at 6000K exhibit a continuous transformation from a dominantly threefold to a mostly fourfold coordination at a higher density regime (about 2.7 to 3.9g/cm^3). The strong dependence of the local structure on density or pressure in *l*-C is an intriguing result and has stimulated experimental investigations. Johnson *et al.* [11] have employed the picosecond time-resolved x-ray absorption spectroscopy to study the bonding of *l*-C and seen that, with increasing density from below 2.0 up to 2.6g/cm^3 , there occurs a change from predominantly *sp*-bonded atomic sites to a mixture of *sp*-, *sp*²- and *sp*³-sites, which is consistent with the first-principles simulation results discussed above.

In this paper, we revisit these interesting and intriguing problems of *l*-C by performing a detail and systematic MD simulation study of the structures and properties of *l*-C as the function of weight density in the range of 1.4 to 3.5g/cm^3 and near the melting curve at 5000 K, using a recently developed accurate three-center TB potential for carbon [12]. Because the *sp*, *sp*² and *sp*³ chemical bonding can be described accurately by the three-center TB model in an equal footing and the TBMD simulations can be performed for larger number of atoms and longer simulation time, the simulations enable us to investigate the details of the competition of these various bonding in the liquid state as the function of the density of the liquid. Our simulation results suggest that liquid carbon in the density range 1.4 to

3.5g/cm³ and near the melting curve at 5000 K can be divided into three distinct phases: a low-density (below 1.9 g/cm³) predominantly *sp* bonding (twofold) liquid, a medium-density (between 1.9 and 3.0 g/cm³) predominantly *sp*² bonding (threefold) liquid, and a high-density (between 3.0 and 3.5 g/cm³) predominantly *sp*³ bonding (fourfold) liquid. The results also indicate that there would be two liquid-liquid phase transitions (LLPT) around the density of 1.9 and 3.0g/cm³ respectively in *l*-C, which is an interesting subject worth further investigations.

The rest of the paper is organized as follows. In section 2, we describe the method of our simulations. In particular, we demonstrate that the TBMD simulations using the three-center TB model have the accuracy comparable to *ab initio* MD simulations, yet much faster. The results of our simulations for *l*-C as the function of density are reported in section 3. Possible LLPT is also discussed. Finally a short summary is given in section 4.

II. Calculation Methods

TB method is an important empirical method, which keeps enough quantum mechanics characteristics of the interatomic interactions while uses the minimal basis set of localized quasiatomic orbitals and parameterized Hamiltonian and overlap matrices. Thus it comprises the accuracy of first-principles methods with the efficiency of classical-potential schemes. The three-center TB potential model for carbon [12] used in the current simulation has been demonstrated to exhibit excellent accuracy and transferability. It describes well the band structures, binding energies and other properties of various carbon crystalline structures, surfaces and clusters. It is also effective enough for large scale MD simulations and can very accurately describe the structures and the dynamical properties of carbon in the liquid state. In Ref. [12], we have shown that the pair-correlation function of *l*-C at 5000K and the density of 2.9g/cm³ obtained from MD simulations using the three-center TB agrees well with that from first-principles MD simulations.

In order to demonstrate the three-center TB potential is accurate and transferable for *l*-C in the range of densities studied in this paper, we also compare the MD simulation results for carbon liquids at 5000K and at three representative densities of 1.7, 2.6 and 3.2g/cm³ respectively using both the three-center TB potential and first-principles density functional theory (DFT). Both simulations for the comparison are performed using a cubic supercell containing 216 atoms with periodic boundary conditions and using Γ point only. The TBMD simulations are performed under constant number of particle, volume, and temperature (NVT) with a time step about 1.4fs. The temperature of the system is controlled by using a stochastic temperature control method to initialize the velocities of the atoms for 2000 MD steps, and then switch to velocity scaling for temperature control. At each density, 15000 MD steps are performed to equilibrate the system and another 10000 MD steps are followed to obtain the atomic trajectories for statistical average and analysis of the structures and properties. The first-principles MD simulations are performed using the VASP code [13]. The calculations are based on

projector augmented-wave (PAW) [14] pseudopotential combined with the generalized gradient approximation [15]. The electronic wavefunctions are expanded in a plane wave basis set with a kinetic energy cutoff of 400 eV. The first-principles MD simulations are performed under NVT ensemble with time step set to 1fs. Nose-Hoover thermostat as implemented in the VASP code is used for the temperature control. At each density, 2000 MD steps are performed to equilibrate the system and another 2000 MD steps are followed to obtain the atomic trajectories for statistical average and analysis of the structures and properties. As one can see from Fig. 1, the pair-correlation functions $g(r)$ and the static structure factors $S(Q)$ of the l -C at three very different densities obtained from our present TBMD simulations are in very good agreement with those from the first-principles MD simulations. This good agreement enables us to perform a systematic TBMD simulation studies of l -C at 5000K over a wide density range with high accuracy.

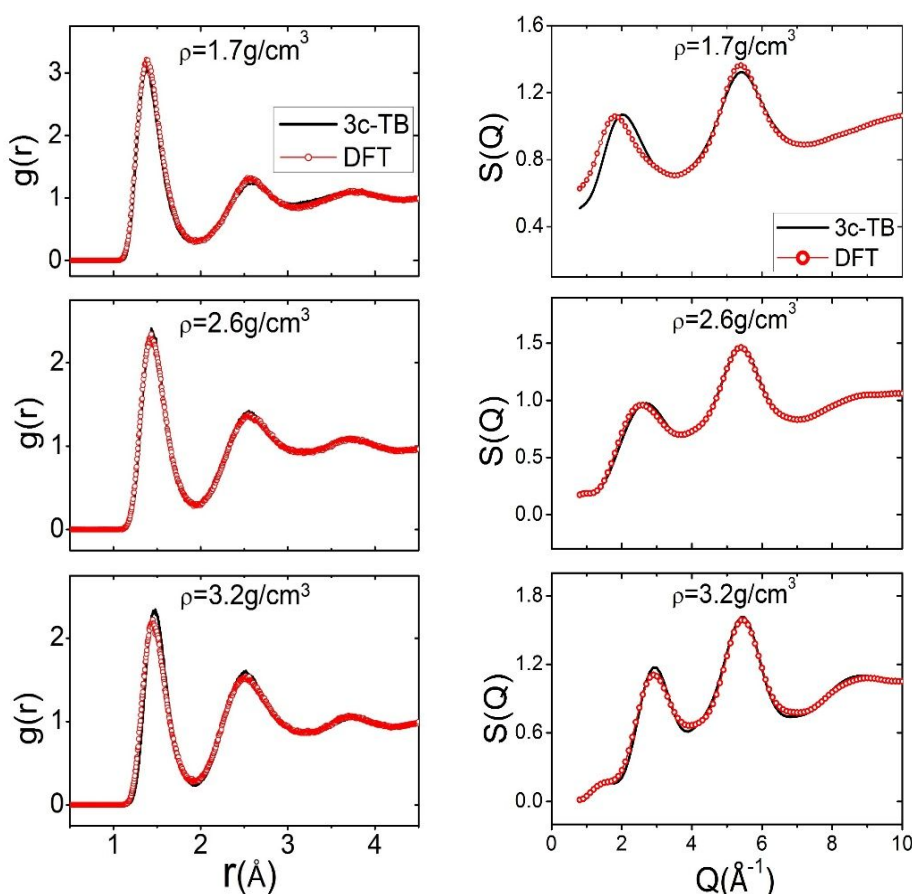


Fig. 1. (Color online) Pair-correlation function $g(r)$ and static structure factors $S(Q)$ for l -C obtained from the TBMD simulations using the three-center TB potential model (black solid line) are compared with the first-principles simulation results (red circle).

In the studies shown below, the TBMD simulations for l -C at 5000K are performed using a cubic

supercell of 512 atoms with periodic boundary conditions. The Γ point only is used to sample the Brillouin zone of our supercell. Since the supercell contains 512 atoms and the atoms are moving around in the liquid state during the MD simulation, Brillouin zone sampling use the Γ point should be sufficient. The length of the computational box is adjusted from 19.4 to 14.3Å to vary the system density from 1.4 to 3.5g/cm³. NVT-MD simulations are performed with a time step about 1.4fs. The thermostat used to control the temperature in our TBMD simulations is to initialize the velocities of the atoms with a stochastic temperature control method for 2000 MD steps, and then switch to velocity scaling for temperature control in the rest of the simulation. At each density, 10000 MD steps are performed to equilibrate the system and another 32000 MD steps are followed to obtain the atomic trajectories for the structures and property analysis. For some higher densities, much longer simulations (up to 100ps) are performed to make sure the liquid is relaxed enough. The quantities of interest, such as pair-correlation function, coordination number, and diffusion coefficient are averaged over all MD steps of simulation at each density.

III. Results and Discussions

In Fig. 2(a), we show the pair-correlation functions $g(r)$ of the *l*-C structures at 5000K obtained from our TBMD simulations, where $g(r)$ s are averaged over 32000 MD simulation steps for each density. For the purpose of clarity, only the results from some selected densities in the LDL, MDL, and HDL respectively are shown in Fig. 2(a). Results from all densities studied in this paper are plotted in Fig. 2(b). It can be seen that the first peak position of the $g(r)$ shifts systematically toward larger distance as the density increased, indicating that the average bond length for nearest neighbor atoms in the liquid increases with density. This behavior is the complete opposite of normal fluids, where one could expect that the neighboring atoms would become more compacted and the position of the first peak in $g(r)$ would decrease as the density increased. More detail of the dependence of the position of the first peak in $g(r)$ on the density (i.e., $R_1(\rho)$) is plotted in Fig. 2(b). It is worth noting that the density range 1.4 to 3.5g/cm³ can be divided into three regions according to slop of $R_1(\rho)$ with respect to the density ρ . The low density region is between 1.4 to 1.9g/cm³ where the $R_1(\rho)$ increases rapidly with ρ from 1.35 to 1.39Å which is smaller than the nearest neighbor distance of sp^2 bonding graphene (1.42Å). The medium density region is between 1.9 to 3.0g/cm³ where the rate of the increase in $R_1(\rho)$ with ρ becomes smaller and $R_1(\rho)$ increases from 1.39 to 1.46 Å with the average R_1 very close to that of the nearest neighbor distance of sp^2 bonding graphene. In the higher density region 3.0-3.5g/cm³, the rate of the increase in $R_1(\rho)$ with ρ is the smallest, with $R_1(\rho)$ changes from 1.46 to 1.48Å, which is about the midway between the graphene bond length and that of the sp^3 bonding diamond structure (1.54Å). At the same time, the height of the first peak in $g(r)$ decreases in the density range 1.4 to 3.0g/cm³, then increases again at higher densities. It is also interesting to note that height of the first peak in $g(r)$ (denoted as $h_1(\rho)$) also exhibits different slops with respect to the density. Below 1.9g/cm³,

the drop of the $h_1(\rho)$ can be well fitted with a linear function with respect to the density. Above 1.9g/cm^3 the variation of $h_1(\rho)$ with respect to ρ is better described by the quadratic function with the minimum about the density of 3.0g/cm^3 . Therefore, the behaviors of the first peak position and height of $g(r)$ as the function of density strongly suggest that there are three distinct types of liquid structure at 5000K and in the density range 1.4 to 3.5g/cm^3 . We refer to three liquid phases as low-density liquid (LDL), medium-density liquid (MDL) and high-density liquid (HDL) as indicated in Fig. 2.

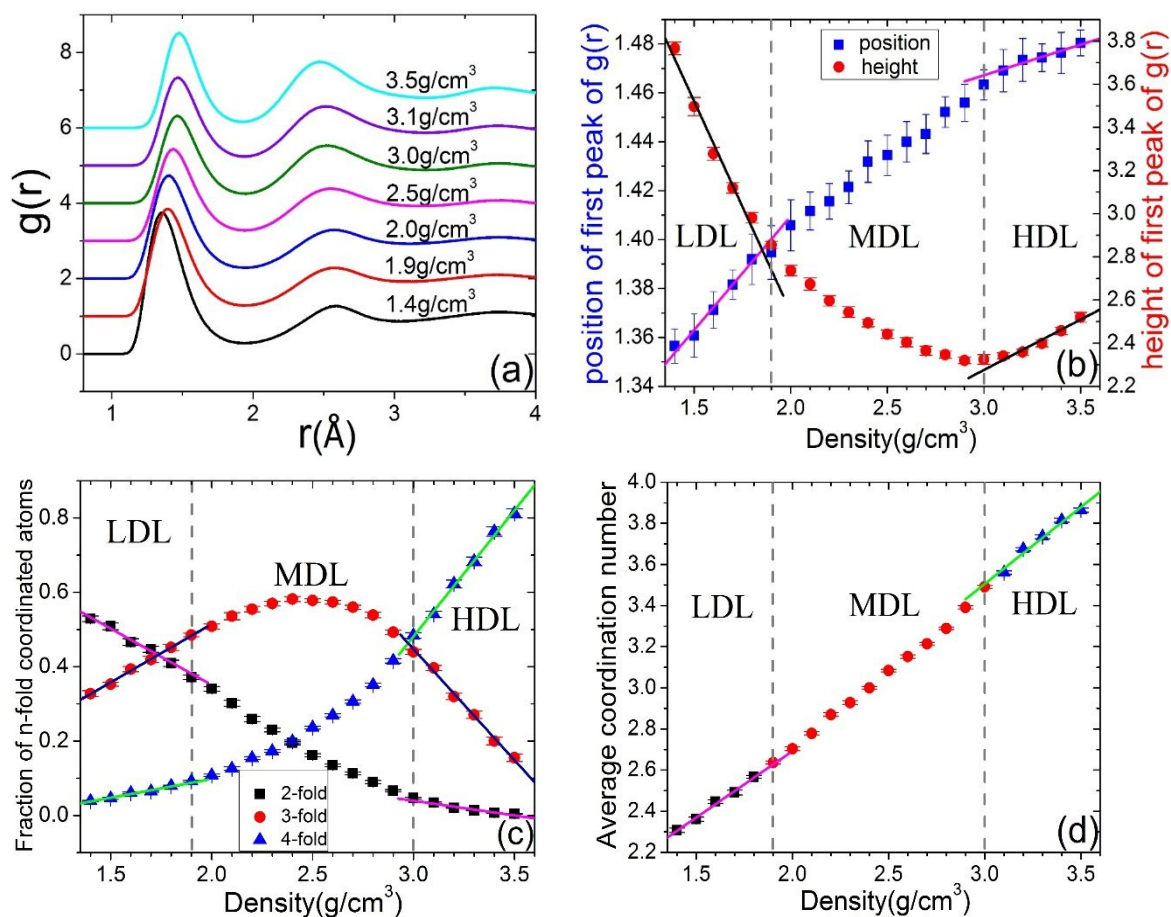


Fig. 2. (Color online) (a) Pair-correlation function $g(r)$ of the l -C structures at 5000 K with the densities of 1.4, 1.9, 2.0, 2.5, 3.0, 3.1 and 3.5 g/cm³. (b) Position ($R_1(\rho)$, blue) and height ($h_1(\rho)$, red) of the first peak in $g(r)$ as a function of density. (c) Fraction of n -fold-coordinated ($n = 2, 3, 4$) atoms and (d) the average coordination number as a function of density. Our calculation results suggest three distinct types of liquid structure which are referred to as low-density liquid (LDL), medium-density liquid (MDL) and high-density liquid (HDL). The separation between LDL and MDL is indicated by the dashed vertical line at 1.9 g/cm³, while that between the MDL and HDL is indicated by the dashed vertical line at 3.0 g/cm³ in Fig. 3(b)-(d).

The structure changes in l -C can be further verified by examining the short-range order (SRO) in the liquid. To this end, we examine the fraction of n -fold-coordinated ($n = 2, 3, 4$) atoms and the average coordination number (CN) as a function of density. The coordination number is calculated by counting the number of atoms in the nearest-neighbor shell whose cut-off radius corresponds to the first minimum of $g(r)$. As shown in Fig. 2(c), at low density, 2-fold-coordinated atoms dominate. With increasing density, the fraction of 3-fold-coordinated atoms increase quickly and reaches a maximum about 60% at about 2.4 g/cm³. At the same time the 2-fold-coordinated fraction decreases quickly and 4-fold coordinated fraction increases quickly. When the density is higher than 3.0 g/cm³, the number of 4-fold-coordinated atoms increases greatly while that of 3-fold-coordinated atoms decreases rapidly. The fraction of 2-fold-coordinated atoms is negligible above 3.0 g/cm³. The variation of the fraction of 2-, 3- and 4-fold coordinated carbon atoms in the liquid as the function of density is consistent with the three liquid forms picture discussed above, although the structural change signals are not strong in the average CN as the function of density shown in Fig. 2(d). The average CN increases almost near-linearly with density. However, some subtle differences in the slope of the average CN with respect to the density in the three liquid regions can be observed. From the coordination number analysis we can see that the LDL, MDL, and HDL are dominated by 2-fold sp -bonding atoms, 3-fold sp^2 -bonding atoms and 4-fold sp^3 -bonding atoms, respectively.

In the literature, the fraction of 2-, 3- and 4-fold coordinated carbon atoms in the liquid of 5000K have been analyzed by first-principles MD simulations at the density of 2.0 g/cm³ [4, 5] and by MD simulations using the “long-range carbon bond order potential” (LCBOPII) model at the density of

1.94g/cm³ [16]. In the first-principles MD simulations, the fraction of 2-, 3- and 4-fold coordinated carbon atoms at the density of 2.0g/cm³ are 0.32, 0.52, and 0.16 respectively. In the LCBOP-II-MD simulations at 1.94g/cm³, these fractions are 0.24, 0.67, and 0.06 respectively. From our TB-MD simulations at the density of 2.0 and 1.9g/cm³, these fractions are 0.34, 0.51, and 0.11 at 2.0g/cm³ and 0.37, 0.49, and 0.09 at 1.90g/cm³, respectively. Clearly, the results from our TB-MD simulations agree well with the first-principles results.

Fig. 3(a) shows the bond-angle distribution functions $P(\theta)$ obtained from our TBMD simulations, where $P(\theta)$ s are calculated for the neighbors within 1.9 Å corresponding to the first minimum of $g(r)$ and averaged over 32000 MD simulation steps for each density. For the purpose of clarity, only the results from some selected densities in the LDL, MDL, and HDL respectively are shown in Fig. 3(a). Results from all densities studied in this paper are plotted in Fig. 3(b). It can be seen that the bond-angle distribution systematically tends to be concentrated at the tetrahedral bond angle of 109.5° as the density increases, indicating that the liquid gets more tetrahedral order at higher density. At low density, the main peak in $P(\theta)$ is very close to 120° but the distribution is broad ranging from 70° to 180°. This suggests some atomic chain-like fragments in LDL. With increasing density, the main peak becomes sharper and shifts to smaller angle, which is consistent with the increase of coordination numbers with the density. Finally $P(\theta)$ takes shape with a peak position of approximately 108° at 3.5g/cm³, which is very close to the tetrahedral angle 109.5°, indicating the formation of the sp^3 bonding structure in HDL. There is also a small peak around 55° in all densities which would be due to the cross links among various coordinated fragments in the liquid samples. More detail of the dependence of the height of the main peak of $P(\theta)$ on the density is plotted in Fig. 3(b). It is worth noting that the slopes of the peak height of $P(\theta)$ with respect to the density at the LDL, MDL and HDL are also different. In short, the changes of $P(\theta)$ with density, which are in accordance with those of $g(r)$ and the fraction n -fold coordinated atoms, also suggest the structural change with density.

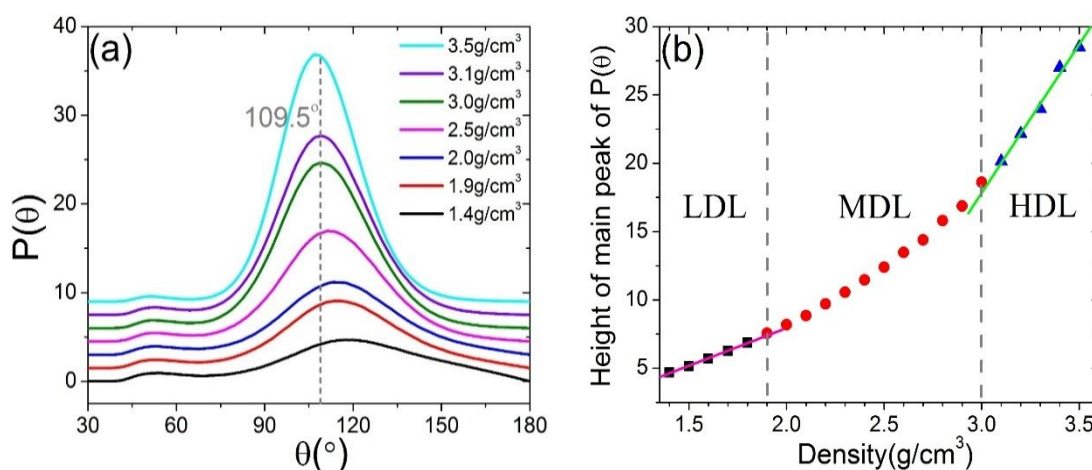


Fig. 3. (Color online) (a) Bond-angle distribution function $P(\theta)$ of the l -C structures at 5000 K with the densities of 1.4, 1.9, 2.0, 2.5, 3.0, 3.1 and 3.5g/cm³. (b) Height of the main peak of $P(\theta)$ as a function of density.

Representative atomic structures of these three liquid phases are shown in Fig. 4, where different colors indicate different coordinated atoms in the liquid. The changes from dominated 2-fold to 3-fold and then to 4-fold atoms and the spatial distribution of different types atoms in *l*-C as the density increases can be seen in the plot. We note that even at the density as low as 1.4g/cm^3 , no voids of significant size are observed.

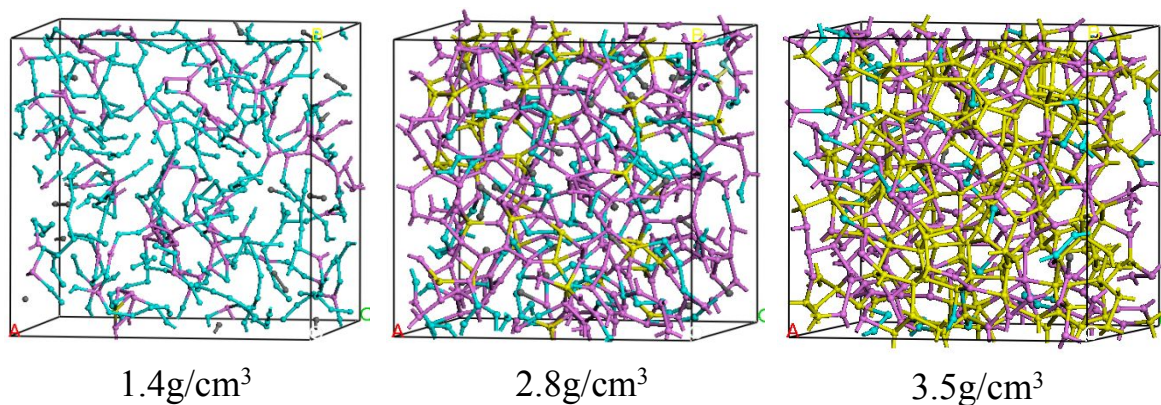


Fig. 4. (Color online) Atomic configuration of *l*-C at densities (a) 1.4g/cm^3 , (b) 2.8g/cm^3 , and (c) 3.5g/cm^3 . The cyan, magenta and yellow represent sp -bond, sp^2 -bond and sp^3 -bond, respectively.

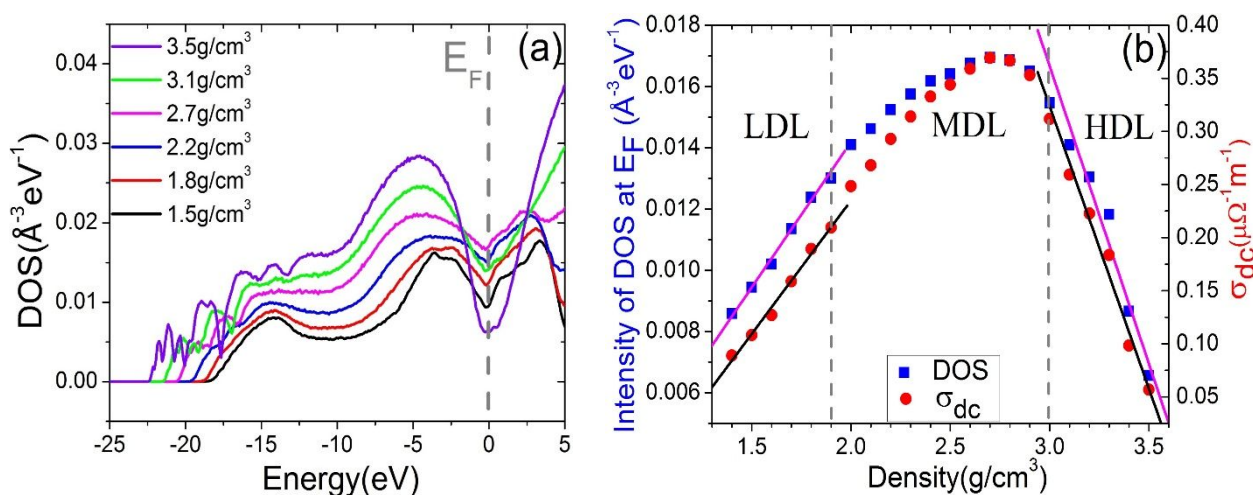


Fig. 5. (Color online) (a) Electronic density-of-states (DOS) of the *l*-C structures at 5000 K with the densities of 1.5, 1.8, 2.2, 2.7, 3.1 and 3.5g/cm^3 . (b) Intensity of DOS at fermi level E_F (blue) and dc conductivity σ_{dc} (red) as a function of density.

The structure and bonding character changes in the liquid are also reflected by their electronic properties. Fig. 5(a) shows the electronic density-of-states (DOS) of the *l*-C structures at some selected densities. More detail of the density dependence of the electronic DOS at Fermi level E_F is plotted in Fig. 5(b). Electronic DOS at E_F is correlated with electronic conductivity of the liquid which can be

probed experimentally. Indeed, the dc conductivity σ_{dc} can be well estimated using the electronic DOS at E_F by the expression [4, 5, 10]

$$\sigma_{dc} = \frac{2\pi\hbar^3 e^2}{m^2} a [N(E_F)]^2, \quad (1)$$

where $N(E_F)$ is the electronic DOS at E_F , and a is a characteristic neighbor distance. The calculated values of σ_{dc} as a function of density are also plotted in Fig. 5(b). From Fig. 5(a) and 5(b) we can see that the electronic DOS at E_F and σ_{dc} increase quickly with the density in the LDL below 1.9g/cm^3 . By contrast, the DOS at E_F and σ_{dc} drop sharply with the increase of density in the HDL. In the MDL, the DOS at E_F and σ_{dc} exhibit a crossover behavior, i.e., they increase in the lower density side (1.9 to 2.7g/cm^3) but decrease in the higher density side (2.7 to 3.0g/cm^3). The behavior of electronic DOS at E_F and σ_{dc} as the function of density is strongly correlated with the structural characteristics changes in the liquid discussed above. In the LDL, the major structure motif is the two-fold chain-like structure which is a good conductor. As the density increases, the cross links between the chains increase therefore the fraction of 3-folded atoms and σ_{dc} increase simultaneously. When the fraction of 3-fold-coordinated atoms reaches the maximum at about 2.3g/cm^3 in the MDL, the fraction of 4-fold-coordinated atoms also grows rapidly and overtakes the 2-fold-coordinated atoms, leading to the reversion of the growth trend in the DOS at E_F and σ_{dc} in the densities 2.7 to 3.0g/cm^3 . In the HDL above 3.0g/cm^3 , 4-fold-coordinated atoms are dominated and a pseudo gap in DOS is formed and σ_{dc} is reduced dramatically as a consequence of the formation of covalent tetrahedral bonding characteristics [17]. Therefore, the trend of electronic DOS at E_F and σ_{dc} verifies again the change of bonding characteristics with density. The strong correlation between σ_{dc} and atomistic structures of the liquid would also provide the mean for experimental probe of the structures of *l*-C at such a high temperature.

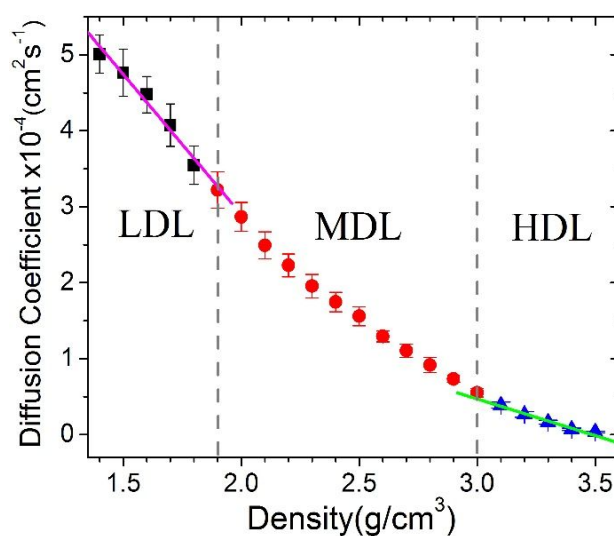


Fig. 6. (Color online) Diffusion coefficient D as a function of density.

We also calculate the diffusion constant of the liquid as the function of the density through the time evolution of the mean square displacement (MSD) $R^2(t)$. All MSDs increases linearly with time, which confirms that our sample is well in liquid state. Furthermore, according to the Einstein relationship

$$D = \lim_{t \rightarrow \infty} \frac{R^2(t)}{6t}, \quad (2)$$

we obtain the diffusion coefficient D from the slope of the MSD, which is presented in Fig. 6. It can be seen that the diffusion coefficient decreases with increasing density. However, the slopes of D vs density in the three liquid phases are different. The change in diffusion constant with density is more rapidly in the LDL, followed by that in the MDL. The variation of D with density in the HDL is much slower. We also note that at the density of 2.0g/cm^3 and the temperature of 5000K , the diffusion constant D $2.9 \times 10^{-4} \text{cm}^2\text{s}^{-1}$ obtained from our TB-MD simulation is very close to the value of $2.4 \times 10^{-4} \text{cm}^2\text{s}^{-1}$ obtained by first-principles MD simulations [4, 5] at the same density and temperature.

An interesting issue related to l -C is whether there is liquid-liquid phase transition (LLPT) when the density or pressure of the liquid varies. Liquid polymorphic phase transitions has attracted continuous attention because of its relevance to the crystal nucleation and crystal-growth process. Pressure-induced first-order LLPT in pure substances have been reported by numerous experimental and theoretical studies [18-23]. For example, LLPT was directly observed in phosphorus by means of *in situ* X-ray diffraction technique [18]. In this experiment, changing the pressure resulted in an abrupt, reversible transformation from low-pressure molecular liquid into the high-pressure polymeric liquid. Group-IV liquids including silicon [19, 20], germanium and tin [20] have also been reported the existence of the pressure-induced structural transition. Being a group-IV element, carbon would be a promising candidate to exhibit pressure-induced LLPT because of its ability to form variety of local bonding. However, the question of LLPT in l -C still a subject of intensive debate despite considerable theoretical, computational and experimental investigations [7-11, 24, 25]. We note that recent experimental measurements, although indirectly, inclined to suggest the existence of LLPT in l -C [11, 24, 25]. The three types of liquid structures at different density regimes observed in our present TBMD simulations are consistent with the scenario of LLPT in liquid carbon. Further thermodynamics calculations, e.g., free energy calculations, to decide whether the LDL to MDL to HDL "transitions" are actually well defined phase transitions would be interesting but would also be challenge.

IV. Conclusion

In summary, with the efficiency and accuracy of the three-center TBMD simulations, we have studied the structural, electronic, dynamical properties of l -C at 5000K with a density range of 1.4 to 3.5g/cm^3 . Our calculation results show that there exist three distinct liquid structures (i.e, LDL, MDL

and HDL) with increasing density, which are dominated by two-fold sp -bonding, three-fold sp^2 -bonding and four-fold sp^3 -bonding atoms, respectively. The structural changes were characterized by the density dependence of the position and height of the first peak in $g(r)$, fraction of the n -fold atoms. The change between the LDL and MDL structures occurs at the density about 1.9g/cm^3 and that between the MDL and HDL structures occurs at the density about 3.0g/cm^3 . The structural changes also manifest themselves in the electronic DOS at E_F , dc conductivity σ_{dc} , as well as diffusion coefficient.

We would like to note that while the second structural change, i.e., the sp^2 MDL to sp^3 HDL, has been widely discussed in the literature, the first changes, i.e., the sp LDL to sp^2 MDL, has been less discussed. In the present paper, only the structural, electronic (DOS and dc conductivity) and dynamics (diffusion) analysis have been performed to characterize the three types of liquids. Although our results present more a smooth than a sharp evolution at the transitions, the results consistently show that the variation of these properties with respect to the density of the system changes the rate (i.e., the slope) around 1.9g/cm^3 and 3.0g/cm^3 respectively, thus provide substantial signals suggesting two phases transitions in this system. The smooth evolution at the transitions would suggest that the transitions are not strong first order phase transition. From the thermodynamics point of view, it would be interesting to calculate the free energy of the liquids in order to clarify whether the LDL to MDL to HDL "transitions" are actually well defined first order phase transitions. However, accurate calculations of free energy to precisely determine the phase transitions in liquid carbon by MD simulations remain very challenging.

Acknowledgments

This work was supported by the U.S. Department of Energy (DOE), Office of Science, Basic Energy Sciences, Materials Science and Engineering Division including a grant of computer time at the National Energy Research Scientific Computing Centre (NERSC) in Berkeley, CA. Ames Laboratory is operated for the U.S. DOE by Iowa State University under Contract No. DE-AC02-07CH11358. Rong Cheng and Wen-Cai Lu were also supported by the National Natural Science Foundation of China (Grant No. 21773132).

References

- [1] M. Togaya, *Phys. Rev. Lett.*, 1997, 79, 2474.
- [2] L.M. Ghiringhelli, J. H. Los, E. J. Meijer, A. Fasolino, and D. Frenkel, *Phys. Rev. Lett.*, 2005, 94, 145701.
- [3] X. F. Wang, S. Scandolo, and R. Car, *Phys. Rev. Lett.*, 2005, 95, 185701.
- [4] G. Galli and R. M. Martin, *Phys. Rev. Lett.*, 1989, 63, 988.
- [5] G. Galli, R. M. Martin, R. Car and M. Parrinello, *Phys. Rev. B: Condens. Matter Mater. Phys.*, 1990, 42, 7470.
- [6] M. P. Grumbach, and R. M. Martin, *Phys. Rev. B: Condens. Matter Mater. Phys.*, 1996, 54, 15730 .
- [7] J. N. Glosli, F. H. Ree, *Phys. Rev. Lett.*, 1999, 82, 4659.
- [8] C. J. Wu, J. N. Glosli, G. Galli, and F. H. Ree, *Phys. Rev. Lett.*, 2002, 89, 135701.
- [9] L. M. Ghiringhelli, J. H. Los, E. J. Meijer, A. Fasolino and D. Frenkel, *Phys. Rev. B: Condens. Matter Mater. Phys.*, 2004, 69, 100101(R).
- [10] J. R. Morris, C. Z. Wang, and K. M. Ho, *Phys. Rev. B: Condens. Matter Mater. Phys.*, 1995, **52**, 4138.
- [11] S. L. Johnson, P. A. Heimann, A. G. MacPhee, A. M. Lindenberg, O. R. Monteiro, Z. Chang, R. W. Lee, and R. W. Falcone, *Phys. Rev. Lett.*, 2005, 94, 057407.
- [12] W.-C. Lu, C. Z. Wang, L.-Z. Zhao, W. Qin, and K. M. Ho, *Phys. Rev. B: Condens. Matter*

Mater. Phys., 2015, 92, 035206.

- [13] G. Kresse and J. Furthmüller, *Phys. Rev. B: Condens. Matter Mater. Phys.*, 1996, 54, 11169;
G. Kresse and D. Joubert, *Phys. Rev. B: Condens. Matter Mater. Phys.*, 1999, 59, 1758.
- [14] P. E. Blöchl, *Phys. Rev. B: Condens. Matter Mater. Phys.*, 1994, 50, 17953.
- [15] J. P. Perdew and Y. Wang, *Phys. Rev. B: Condens. Matter Mater. Phys.*, 1992, 45, 13244.
- [16] F. Colonna, J. H. Los, A. Fasolino, and E. J. Meijer, *Phys. Rev. B: Condens. Matter Mater. Phys.*, 2009, 80, 134103.
- [17] S. S. Ashwin, U.V. Waghmare, and S. Sastry, *Phys. Rev. Lett.*, 2004, 92, 175701.
- [18] Y. Katayama, T. Mizutani, W. Utsumi, O. Shimomura, M. Yamakata and K. Funakoshi, *Nature*, 2000, 403, 170.
- [19] N. Funamori and K. Tsuji, *Phys. Rev. Lett.*, 2002, 88, 255508.
- [20] K. Tsuji, T. Hattori, T. Mori, T. Kinoshita¹, T. Narushima¹ and N. Funamori, *J. Phys.: Condens. Matter*, 2004, 16, S989.
- [21] S. Falconi, L.F. Lundegaard, C. Hejny, M. I. McMahon, *Phys. Rev. Lett.*, 2005, 94, 125507.
- [22] S. Falconi, G.J. Ackland, *Phys. Rev. B: Condens. Matter Mater. Phys.*, 2006, 73, 184204.
- [23] N. Jakse and A. Pasturel, *Phys. Rev. Lett.*, 2007, 99, 205702.
- [24] D. Kraus, J. Vorberger, D. O. Gericke, V. Bagnoud, A. Blažević, W. Cayzac, A. Frank, G. Gregori, A. Ortner, A. Otten, F. Roth, G. Schaumann, D. Schumacher, K. Siegenthaler, F. Wagner, K. Wünsch, and M. Roth, *Phys. Rev. Lett.*, 2013, 111, 255501.
- [25] A. M. Kondratyev, V. N. Korobenko and A. D. Rakhel, *J. Phys.: Condens. Matter*, 2016, 28, 265501.